Journal of Medicinal Chemistry

pubs.acs.org/jmc

Article

Open Access

This article is licensed under CC-BY-NC-ND 4.0

Discovery of Cell-Permeable Macrocyclic Cyclin A/B RxL Inhibitors that Demonstrate Antitumor Activity

Andrew T. Bockus,‡ Siegfried S. F. Leung,‡ Breena Fraga-Walton, Miguel P. Baldomero, Luis Hernandez, Nathan J. Dupper, Justin A. Shapiro, Bryan M. Lent, David C. Spellmeyer, Megan K. DeMart, Joshua Luna, Dalena Hoang, Manesh Chand, Yuliana Gritsenko, Cayla McEwen, Mahesh Ramaseshan, Catherine E. Gleason, Frances Hamkins-Indik, Miles W. Membreno, Jie Zheng, Ranya Odeh, Meisam Nosrati, Daphne He, Ramesh Bambal, Peadar Cremin, Jinshu Fang, Bernard Levin, Evelyn W. Wang, Marie Evangelista, David Earp, Constantine Kreatsoulas, Rajinder Singh, Pablo D. Garcia, and James B. Aggen*

Cite This: J. Med. Chem. 2025, 68, 17030−17045

Read Online

ACCESS | Metrics & More | Article Recommendations | Supporting Information

ABSTRACT: The cyclin-dependent kinase (CDK)/retinoblastoma protein (RB)/early region 2 binding factor (E2F) axis forms the core transcriptional machinery driving cell cycle progression. Alterations in *RB1* or other pathway members occur in many cancers, resulting in heightened oncogenic E2F activity. The activity of E2F is regulated by RxL-mediated binding to the hydrophobic patch (HP) of Cyclin A; blocking this interaction results in the hyperactivation of E2F and synthetic lethality in E2F-driven tumors. While mechanistically differentiated and potentially more selective than blocking CDK activity (e.g., CDK2 or CDK4 inhibitors), the Cyclin A/E2F RxL interaction was deemed undruggable. Utilizing structure-based design, we have discovered a family of cell-permeable macrocyclic Cyclin A/B RxL inhibitors that show potent and selective activity against *RB1/E2F*-dysregulated cancer cell lines. Lead compound **34** demonstrated proof-of-concept efficacy via intraperiotoneal (IP) administration in mouse cell line-derived xenograft (CDX) tumor models.

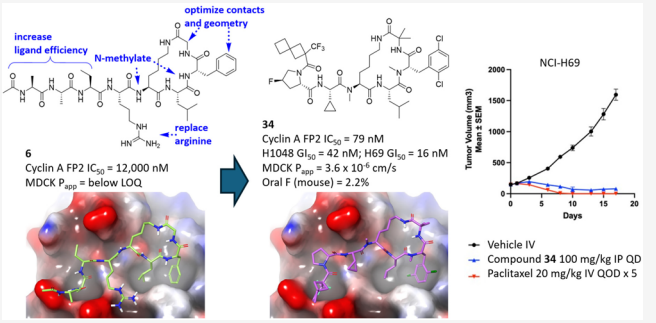

Downloaded via 66.179.154.202 on May 6, 2026 at 22:09:28 (UTC).
See https://pubs.acs.org/sharingguidelines for options on how to legitimately share published articles.

INTRODUCTION

Cyclins are intracellular regulatory proteins that bind and activate their cognate Cyclin-Dependent Kinases (CDKs) to regulate phase-specific activities, important checkpoints, and orderly phase transitions through the cell cycle (Figure 1).[1] Alterations in the cell cycle machinery are common features of cancers,[2] making Cyclin/CDK complexes attractive targets for drug development.[3] Because kinases contain small three-dimensional catalytic binding pockets,[4] they are very tractable targets for traditional small-molecule inhibitors.[5] Indeed, several CDK inhibitors with diverse selectivity have been approved for clinical use.[3,6] However, CDK inhibitors are limited both by the development of resistance[7] and off-target effects that are due to the high structural homology of the catalytic site across kinases.[8] Cyclins, on the other hand, have been historically considered to be undruggable because they lack a discrete active site. Cyclin/CDK complexes, however, recruit some substrates via a protein−protein interaction (PPI) between the hydrophobic patch (HP), formed by the MRAIL motif of the Cyclin and the RxL motif of the respective substrate (Figure 1).[9−11] Thus, a direct inhibitor of Cyclin-mediated PPIs with substrates could theoretically provide comparable therapeutic benefits to targeting kinases directly while circumventing some of the drawbacks of small-molecule CDK inhibitors.[12]

Pioneering work by Kaelin and co-workers demonstrated that Cyclin/CDK2 inhibition is synthetically lethal with retinoblastoma (Rb) dysregulation and high levels of E2F expression, which is widespread in many types of difficult-to-treat cancers, including small-cell lung cancer (SCLC).[13] They hypothesized that by preventing the interaction with Cyclin A/Cdk2 and the inhibitory phosphorylation of E2F, its activity was further increased and maintained beyond the S phase, ultimately resulting in apoptosis. This was directly demonstrated with a peptide derived from the RxL motif of p27

Received: January 24, 2025
Revised: April 22, 2025
Accepted: May 5, 2025
Published: August 14, 2025

ACS Publications

© 2025 American Chemical Society

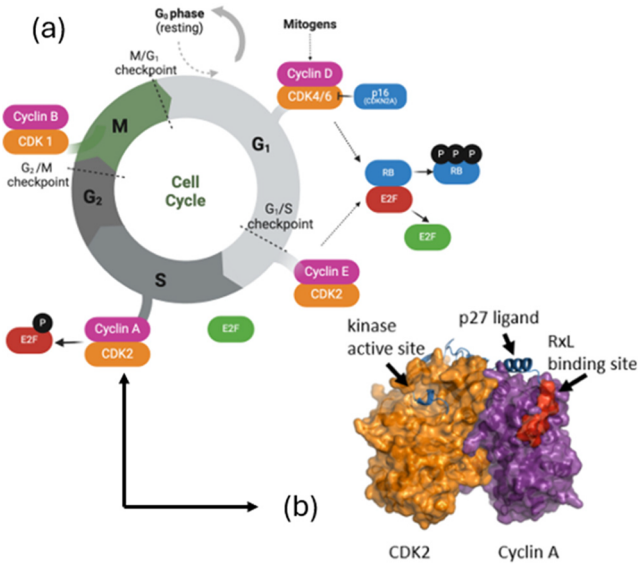

Figure 1. (a) Cell division cycle depicting CDK/Cyclin complexes that regulate the phosphorylation state of retinoblastoma (Rb) and early region 2 binding factor (E2F). (b) Structure of the CDK2/Cyclin A complex bound to p27 (PDB: 1JSU), highlighting the RxL motif of p27 (in red) bound to the hydrophobic patch of Cyclin A.[11]

conjugated to a cell-penetrating trans-activator of transcription (TAT) motif, which selectively induced apoptosis in transformed cell lines with a high expression of E2F and not in normal cells. These results suggested that a potential therapeutic benefit could be achieved by direct inhibition of this Cyclin-RxL-mediated PPI. However, the relatively large and shallow nature of this protein−protein interaction site poses a challenge for the development of traditional small-molecule inhibitors. In addition, the conserved arginine residue in the RxL motif, which forms a salt-pair with the Cyclin, could limit the potential for the discovery and development of passively cell-permeable inhibitors.[14−17]

We leveraged computational modeling and semiautomated solid-phase synthesis to discover cell-permeable macrocyclic peptides targeting the Cyclin A HP:RxL interaction. We approached this target with a "permeability-first" philosophy, anticipating that the success of an intracellular peptide drug discovery program is best served by intentionally optimizing both permeability and biochemical potency simultaneously at all stages of a program.[18] A fragment of the naturally occurring Cyclin A/CDK2 inhibitor p27 that contained the RxL motif provided an attractive starting point, as the cocrystal structure of p27 bound to Cyclin A/CDK2 offered insights into the binding interactions and conformation of this region.[16]

We recognized early on in this project that replacing the conserved arginine residue would be required to identify cell-permeable inhibitors of Cyclin A and that the modification may also lead to improved oral absorption of these macrocycles. One indication of the negative impact of arginine on the oral absorption of peptide macrocycles can be seen by comparing two analogous macrocyclic peptides: desmopressin, which has a D-arginine residue at position 8 in the tail, demonstrates 0.16% oral bioavailability in humans, while oxytocin, which has a leucine residue at that position, demonstrates 4.4% oral bioavailability in humans.[19,20] Oral bioavailability has been achieved with highly basic and zwitterionic compounds within the rule-of-five (Ro5) physicochemical space, possibly by leveraging active transport or paracellular transport mechanisms,[21,22] but oral absorption beyond the rule-of-five space has been historically challenging for macrocycles.[5] We postulated that we could access passively permeable macrocyclic inhibitors by first eliminating the conserved arginine residue and then compensating for the subsequent loss of affinity by exploiting surface-exposed H-bonds and hydrophobic interactions within the relatively shallow cavities of the Cyclin A HP.

We began by first identifying cell-permeable scaffolds that are amenable to substitution within the context of our target site. In parallel, we identified features that imparted affinity in our biochemical assays and then grafted these moieties onto the permeable scaffolds to produce permeable compounds with measurable cellular activity. Once permeable hits were identified, we applied a traditional structure-based design coupled with property optimization adherent to beyond rule-of-five (bRo5) drug-likeness criteria in order to achieve a balance of potency, permeability, and physicochemical properties.[23−25] Using this approach, we were able to successfully develop a nanomolar peptidic macrocycle inhibitor of Cyclin A/B that demonstrates 2.2% oral bioavailability and tumor regression in small-cell lung cancer mouse xenograft models. Further optimization of the potency and oral bioavailability of this class of compounds resulted in the identification of CID-078, a first-in-class, orally bioavailable Cyclin A/B inhibitor, currently being evaluated in patients with advanced solid tumor malignancies.[26]

RESULTS

Binding Model and Chemistry Strategy. To establish a binding model from which to base our design hypotheses, we focused on the Cyclin A HP:RxL interaction site within the published crystal structure of p27 in complex with Cyclin A/Cdk2 (PDB ID: IJSU).[27] The key interactions, as illustrated in Figure 2, can be characterized by (1) the hydrophobic interactions at two sites: the hydrophobic patch (HP), in which Leu32 of the RxL motif binds, and an adjacent secondary hydrophobic pocket (S), which is N-terminal to the conserved Arg30 of p27; (2) the extended hydrogen bonding network between the backbone of p27 and Cyclin A; and (3) the salt bridge interaction between Arg30 of the RxL motif and Glu220 of Cyclin A. As previously reported,[28] we developed a binding model for lariat macrocycles based on the Cyclin A-bound crystal structures of p27 (PDB: 1JSU, pink in Figure 2A) and a previously published lariat macrocycle (PDB: 1URC, yellow),[27,29] to facilitate structure-based design (SI Figure S1). We synthesized compound **6** (compound "5a" in original publication), which displayed an IC_{50} of 0.77 μM in our Cyclin A **FP1** assay and an immeasurably low cell permeability (MDCK P_{app} = below limit of quantitation (LOQ)).[27] Previous reports have shown that with **6**, and closely related series, the replacement of the arginine with neutral moieties results in the complete ablation of biochemical activity.[27]

To efficiently develop both structure−activity and structure−permeability relationships, all discovery-scale compounds reported here were synthesized using our in-house semi-automated solid-phase peptide synthesis platform. Linear sequences were synthesized on 2-chlorotrityl chloride resin using a 48-vial Biotage Syro II synthesizer (Scheme 1) with automated site-specific *N*-methylation introduced as needed.[30] Linear products were cleaved from the solid phase and cyclized

https://doi.org/10.1021/acs.jmedchem.5c00253
J. Med. Chem. 2025, 68, 17030−17045

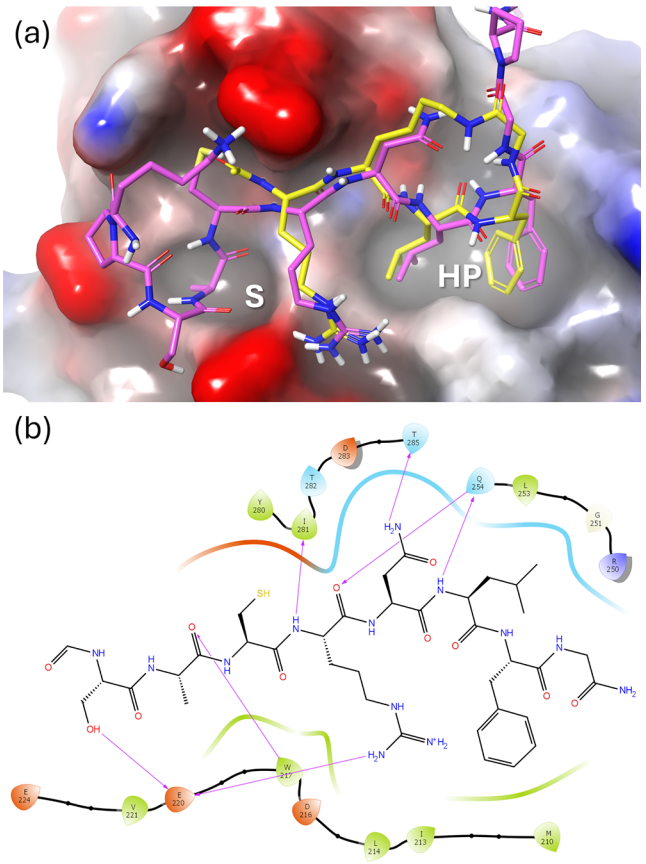

Figure 2. Cyclin A Hydrophobic Patch (HP):RxL Interaction Site. (a) Overlay of bound ligands, including p27 (pink, PDB: 1JSU) and a lariat macrocycle (yellow, PDB: 1URC), at the interaction site (surface representation colored by electrostatic potential, PDB: 1JSU). (b) Ligand interaction diagram of the Cyclin A-bound p27 peptide (PDB: 1JSU). Hydrogen bonds are shown with purple arrows.

in solution. Cyclized products were then purified via HPLC, yielding 1−10 mg of each compound with >95% purity. This synthetic strategy was particularly powerful for exploring both side chain and backbone structure activity relationship (SAR) in a modular fashion, as it allowed for site-selective backbone N-alkylation with a variety of alkyl donors, thereby greatly increasing the diversity accessible while using a limited number of building blocks.

Determining Structural Requirements for Passive Cell Permeability. Cell permeability has been a key challenge in developing macrocycle therapeutics.[31,32] While much work has been published on the structural relationships of permeability of head-to-tail macrocycles, primarily cyclic penta- and hexa-peptides,[31,33−37] relatively little is known about the permeability properties of sidechain-to-tail cyclized lariats.[38] Composed of a macrocyclic portion referred to herein as the "macrocyclic core" and an unconstrained exocyclic sequence referred to as a "tail", lariat structures have more degrees of freedom than traditional head-to-tail (homodetic) macrocycles. Furthermore, the potential intramolecular hydrogen bonding (IMHB) interactions between the macrocyclic core and tail add complexity to the understanding of how such structures permeate membranes.[39]

We devised a strategy to identify permeable binders of Cyclin A HP starting with the scaffold of **6**. Focusing first on optimizing the permeability of the macrocyclic core, we designed a truncated lariat series with a tail composed of a single lipophilic residue (Table 1). In accordance with the design principles of permeable cyclic peptides, our designs sampled various backbone *N*-methylation. The backbone amide NHs of Arg and Leu of the RxL motif were shown to participate in the hydrogen bonding network at the binding interface (Figure 2), and thus, the corresponding amide NHs in the truncated series were not methylated. The backbone amide of the phenylalanine, on the other hand, was expected to be solvent-exposed, and modeling suggested that backbone *N*-methylation at this position would be tolerated (Table 2). Therefore, Phe was *N*-methylated in this series.

Initially, we found that compounds with Gly at R_4 (**1** and **2**) demonstrated poor permeability regardless of their *N*-methylation count, suggesting that other characteristics of the parent lariat scaffold might contribute to poor intrinsic permeability (Table 1). The R_4 Gly residue was replaced with D-norvaline (D-Nva) to both increase the lipophilicity and potentially alter the conformation of the scaffold. Based on our

Scheme 1. Generalized Approach to Solid-Phase Peptide Synthesis of RxL-Mimicking Lariat Macrocycles[a]

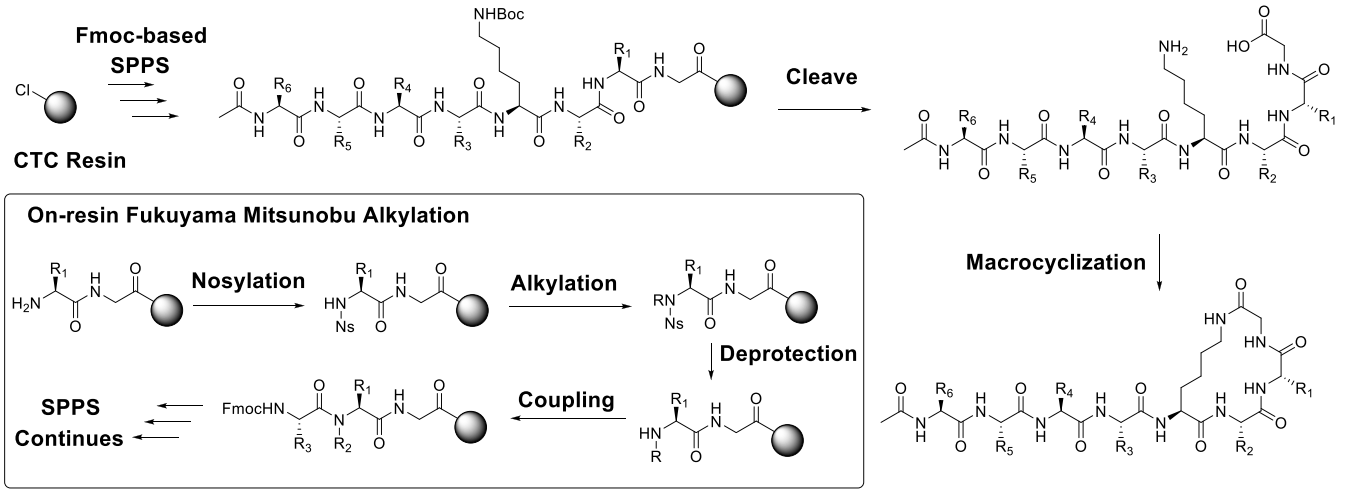

[a](Inset) Generalized sequence for on-resin alkylation of amines via an automated Fukuyama-Mitsunobu reaction.

https://doi.org/10.1021/acs.jmedchem.5c00253
J. Med. Chem. 2025, 68, 17030−17045

Table 1. Permeable Macrocyclic Cores Identified via *N*-Methylation and Side-Chain Scanning

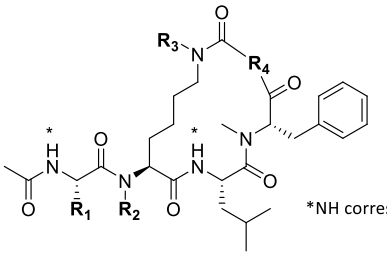

ID	R_1	R_2	R_3	R_4	#NMe	#HBD	#HBA	MW	ALogP	PSA	ΔG_{Insert}	MDCK P_{app} A-B (x10-6 cm/s)
1		H	H		1	5	6	614.8	1.0	166	14.1	0.3
2		CH_3	CH_3		4	2	6	670.9	2.5	139	6.82	0.6
3		CH_3	H		2	4	6	684.9	2.9	157	7.08	1.1
4		H	CH_3		2	4	6	684.9	2.9	157	8.06	0.2
5		CH_3	CH_3		3	3	6	698.9	3.3	148	5.18	14.9

Table 2. Virtual Design of Compound 6 Analogues Identifies Features to Improve Biochemical Affinity[a]

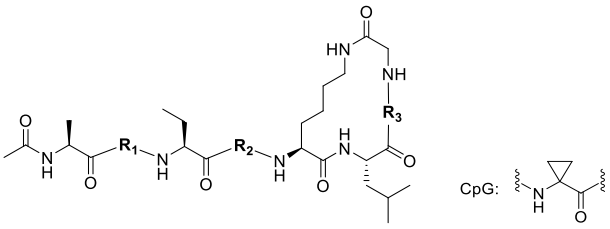

ID	R_1	R_2	R_3	Glide SP Docking Score	MMGBSA ΔG_{Bind} (kcal/mol)	CycA FP1 IC_{50} (μM)	MDCK P_{app} A-B ($x10^{-6}$ cm/s)
6	L-Ala	L-Arg	L-Phe	-11.4	-86.7	0.77	Below LOQ
V1	CpG	L-Arg	L-Phe	-11.4	-88.9	N/A	N/A
V2	L-Ala	L-Leu	L-Phe	-10.4	-79.0	N/A	N/A
V3	L-Ala	L-Arg	NMe-L-Phe	-11.9	-90.2	N/A	N/A
V4	L-Ala	L-Arg	L-2Cl-Phe	-11.8	-94.4	N/A	N/A
V5	L-Ala	L-Arg	L-3Cl-Phe	-11.5	-91.7	N/A	N/A
7	L-Ala	L-Leu	NMe-L-Phe	-10.4	-82.4	55.3	0.3

[a]N/A = Not Acquired.

model, the D-Nva side chain was predicted to point away from the protein; thus, it was expected not to interfere with target binding. The D-Nva-containing compounds displayed a range of Madin-Darby canine kidney (MDCK) permeabilities dependent on the number and pattern of *N*-methylation. While methylation of the Nα-Lys (**3**, MDCK $P_{app} = 1.1 \times 10^{-6}$ cm/s) was shown to drive a much larger improvement to permeability than did the *N*-methylation of the Nε-Lys (**4**, MDCK $P_{app} = 0.2 \times 10^{-6}$ cm/s), di-*N*-methylation of both Nα-Lys and Nε-Lys resulted in the highly permeable **5** (MDCK $P_{app} = 14.9 \times 10^{-6}$ cm/s). Compounds **3** and **5** were identified as the most viable *N*-methylated scaffolds with which to initiate our cell-permeable hit generation campaign.

Increasing the hydrophobicity effectively enhanced the permeability in this macrocycle series. The general trend can be captured by molecular descriptors, such as AlogP, polar surface area (PSA), and number of hydrogen-bond donors (#HBD), as well as the computed free energy of membrane insertion (ΔG_{insert}),[40] which estimates the free energy cost of membrane partition from the predicted conformation in a low-dielectric environment (Table 1). The permeability difference between **3** and **4**, a structural isomer pair with different *N*-

https://doi.org/10.1021/acs.jmedchem.5c00253
J. Med. Chem. 2025, 68, 17030−17045

Table 3. Optimization of N-Terminal Tail Rescues Biochemical Activity[a]

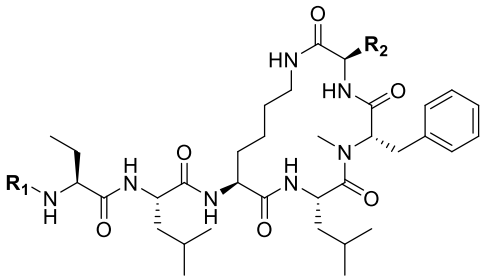

ID	R_1	R_2	ALogP	CycA FP1 IC_{50} (μM)	MDCK P_{app} A-B ($x10^{-6}$ cm/s)
7	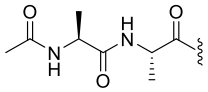	H	-0.1	55.3	0.3
8	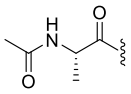	H	0.4	25.0	N/A
9	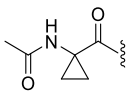	H	0.6	3.78	N/A
10	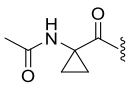	$-CH_2CH_2CH_3$	1.8	7.75	N/A
11	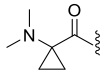	$-CH_2CH_2CH_3$	2.2	1.51	N/A
12	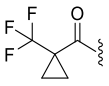	$-CH_2CH_2CH_3$	3.4	0.99	0.6

[a]N/A = Not Acquired.

methylation patterns, as reflected by the ΔG_{insert} values, suggests conformational effects, such as intramolecular hydrogen bonding or shielding, also contribute to the permeability characteristics.

Achieving Cyclin A Biochemical Activity in the Context of Permeability-Compatible Features. We modeled a series of virtual designs based on compound **6** to identify positions where modification may improve binding affinity and potential permeability (Table 2). Utilizing the Cyclin A cocrystal structures, we computed the binding poses to Cyclin A by docking,[28] followed by molecular mechanics generalized Born surface area (MM-GBSA) postscoring. Replacing Arg with Leu at R_2 was predicted to be unfavorable (**6** and **V2**), consistent with the loss of a key salt bridge to Cyclin A Glu220 (Figure 2). α-Substitution of R_1 (**V1**) to better fill the S pocket and *N*-methylation or a chlorine substituent on Phe (**V3**−**V5**) to better fill the HP pocket with the added hydrophobic moieties were predicted to be constructive. We subsequently synthesized and tested **7**, a neutral compound containing the Arg to Leu replacement as well as NMe-L-Phe that was predicted to be favorable for binding. In reasonable agreement with binding predictions (ΔSP docking score = 1.0; ΔMM-GBSA ΔG_{bind} = 4.3 kcal/mol), the neutral analogue **7** showed weak but measurable activity in the CycA **FP1** assay (IC_{50} = 55 μM), approximately 70-fold activity loss (~2.4 kcal/mol@298 K) relative to the Arg-containing **6** (IC_{50} = 0.77 μM). Importantly, **7** also showed improved permeability relative to parent compound **6**, achieving low but measurable MDCK permeability.

We then designed a series of peptides based on compound **7** with the aim of restoring activity to the scaffold while incorporating only permeability-compatible features (Table 3). We first endeavored to increase the ligand efficiency of **7** by optimizing contacts between the N-terminal tail and the secondary hydrophobic pocket (pocket S, as shown in Figure 2). The N-terminal Ala residue is predicted to be mostly solvent-exposed in the computed binding model (Figure 3), and shortening of the polypeptide tail by one residue in compound **8** was tolerated as expected. Subsequently, substituting the methyl side chain for a 1,1′-aminocarboxylcyclopropyl moiety, which was predicted to improve interactions with the S pocket, resulted in an order-of-magnitude improvement in biochemical affinity for compound **9**. Replacing the Gly residue with D-Nva in the macrocycle core was well tolerated, as anticipated in compound **10**, providing a new macrocycle scaffold for optimization. Based on the assumption that the cyclopropyl moiety of the lariat's tail fills the S pocket, a basic moiety at the N-terminus was expected to be beneficial for binding in the presence of Glu220 and Glu224 peripheral to the S pocket. The basic dimethylamine analogue, compound **11**, while incompatible with our permeability aims, was made to test this binding hypothesis, and the resulting 4-

https://doi.org/10.1021/acs.jmedchem.5c00253
J. Med. Chem. 2025, 68, 17030−17045

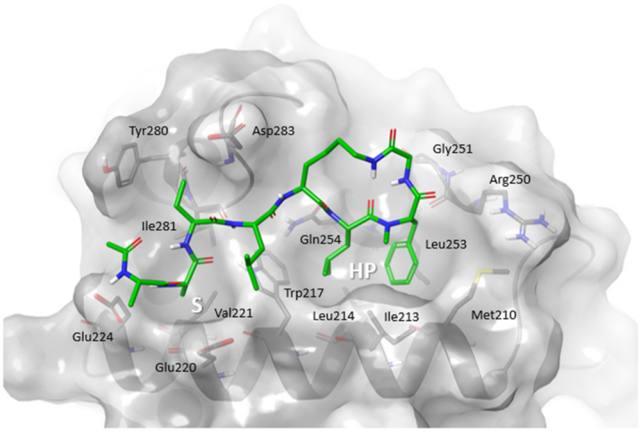

Figure 3. Model of compound 7 bound to Cyclin A. Compound 7 is assumed to bind similarly to the p27 peptide (Figure 2a), filling both the HP and S pockets while maintaining an extensive hydrogen bonding network with Cyclin A in the absence of the Arg residue.

fold improvement in biochemical activity supported our binding model. The replacement of the terminal basic amine with a trifluoromethyl group in compound **12** improved activity to a level equivalent to that of the Arg-containing reference compound **6**. Conformational analysis of **12** indicates that we restricted its conformational space to readily sample the bioactive structure (SI Figure S2). As anticipated, compound **12**, with its smaller size and higher calculated hydrophobicity, demonstrated improved permeability compared to that of the bigger and more polar compound **7**.

Identification of Cell-Active Hits by Combining Permeability and Activity SAR. To better assess progress in improving the potency of Cyclin A inhibitors, we introduced a second-generation assay ("**FP2**") with a higher affinity fluorescence polarization (FP)-probe. The apparent K_d values for cyclin A/CDK2 with the original **FP1** probe and the new **FP2** probe were 7.4 and 1.1 nM, respectively. The higher affinity **FP2** probe resulted in improved potency resolution using **FP2** for compounds with IC_{50} < 1 μM since inhibitors required higher affinity to displace the probe and because lower concentrations of Cyclin A/Cdk2 could be used. In this assay, we found that the reference compound **6** showed a CycA **FP2** IC_{50} of 12.7 μM, as compared to its CycA IC_{50} of 0.77 μM in the **FP1** assay. Based on the structural understanding that both meta- and ortho-substituted phenylalanine could further enhance permeability and potency (Table 2 and SI Table S3), we set out to combine the best features from each prior subseries to identify compounds with cellular activity. As initially hypothesized, *N*-methylation patterns that yielded permeable macrocyclic core scaffolds with a truncated tail (Table 1) had analogous effects in our combination series that included a full-length tail (Table 4). We combined the tail of compound **12** (Table 3) with a 3-chloro-substituted phenylalanine (**V5**, Table 2) and the moderately permeable *N*-methylation pattern of compound **3** (Table 1) in hybrid compound **13** (Table 4), which demonstrated comparable permeability and superior affinity for the target (CycA **FP1** IC_{50} = 0.23 μM; CycA **FP2** IC_{50} = 2.05 μM) relative to that of compound **12**. Comparing results for **13** to **6** also demonstrated that we had not only recovered but improved the affinity for Cyclin A by using an intrinsically permeable scaffold that lacked arginine residues. Importantly, we also found that relative permeability ranking translated from the inactive truncated scaffolds in Table 1 to the bioactive scaffolds in Table 4. As expected, compound **14**, which shares the same *N*-methylation pattern as found in weakly permeable compound **4** (Table 1), was also poorly permeable. Compound **16** (Table 4), on the other hand, which combines the linear tail of compound **12**, a 2,5-dichlorophenylalanine, and the highly permeable tri-*N*-methyl macrocycle from compound **5** (Table 1), demonstrated high passive permeability (MDCK P_{app} = 19.6 × 10^{-6} cm/s). We were encouraged to see, for the first time in the pursuit of this target, weak but measurable growth inhibition of the NCI-H1048 small cell lung cancer line upon incubation with multiple compounds (Table 4). While this exercise validated the viability of our permeability-first approach, significant hit-to-lead optimization was still required to arrive at molecules for in vivo proof-of-concept.

Hit-to-Lead Optimization. In the hit-to-lead phase, we aimed to (1) further improve biochemical affinity and cellular potency, (2) maintain passive permeability, (3) balance physicochemical properties, (4) monitor selective cytotoxicity by demonstrating the NCI-H1048 Rb-dysregulated cell line is

Table 4. Cell-Permeable Hits Identified by Combining Permeable and Active Features[a]

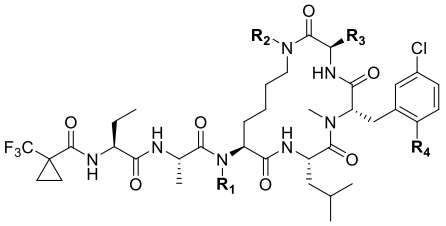

ID	R_1	R_2	R_3	R_4	ALogP	CycA FP1 IC_{50} (μM)	CycA FP2 IC_{50} (μM)	H1048 GI_{50} (μM)	WI-38 GI_{50} (μM)	MDCK P_{app} A-B ($\times 10^{-6}$ cm/s)
13	CH_3	H	$-CH_2CH_2CH_3$	H	3.4	0.35	2.05	6.85	≥ 9.9	0.5
14	H	CH_3	$-CH_2CH_2CH_3$	H	3.4	0.30	3.06	N/A	N/A	Below LOQ
15	CH_3	H	$-CH_2CH_2CH_3$	Cl	4.0	0.16	1.39	6.65	≥ 20	2.1
16	CH_3	CH_3	$-CH_2CH_3$	Cl	4.0	0.39	1.23	N/A	N/A	19.6

[a]N/A = Not Acquired.

https://doi.org/10.1021/acs.jmedchem.5c00253
J. Med. Chem. 2025, 68, 17030−17045

Table 5. 100× Improvement in GI_{50} Achieved via Introduction of Fluoroproline Residue[a]

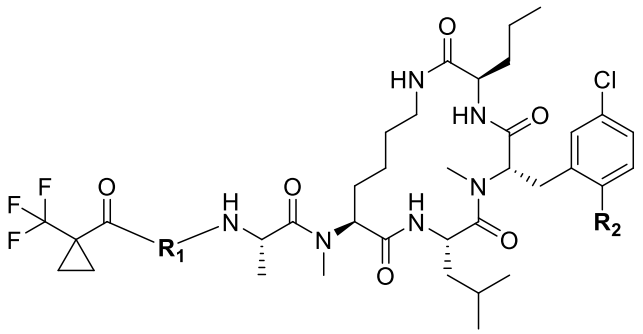

ID	R_1	R_2	ALogP	CycA FP2 IC_{50} (μM)	CycB FP2 IC_{50} (μM)	CycE FP2 IC_{50} (μM)	H1048 GI_{50} (μM)	WI-38 GI_{50} (μM)	MDCK P_{app} A-B (10^{-6} cm/s)
13		H	3.4	2.05	0.047	6.37	6.85	≥ 9.9	0.5
17		H	3.5	1.90	0.030	≥ 20	3.35	≥ 20	0.3
15		Cl	4.0	1.39	0.072	13.0	6.65	≥ 20	2.1
18		Cl	4.1	1.09	0.027	16.5	2.24	≥ 20	2.7
19		Cl	4.1	0.232	≤ 0.020	2.27	0.066	≥ 20	1.0

[a]N/A = Not Acquired.

uniquely sensitive to our compounds compared to WI-38 nontransformed fibroblasts, and (5) identify drivers of Cyclin selectivity. We introduced several new assays to monitor our progress, including second-generation Cyclin B and E FP ("**FP2**") assays, which use the same probe as the Cyclin A **FP2** assay, to improve our ability to rank compound affinities and cross-Cyclin activities.

We attempted to design a compound with improved biochemical affinity and cellular activity by further biasing the preferred conformation of the backbone toward that observed in the putative binding model (SI Figures S1−S3). Our models suggested that a Pro residue at the R_1 position (Table 5) would reduce conformational freedom to promote projection of the N-terminal trifluoromethylcyclopropyl residue into the S pocket, orient its backbone carbonyl to productively hydrogen bond with the side chain of Trp217, and eliminate a nonessential hydrogen-bond donor from the peptidic backbone. Using compound **13** as a starting point, we substituted a proline moiety in place of the Abu residue at residue R_1 to provide compound **17**. Unexpectedly, this modification did not significantly improve either potency or permeability. In a parallel series, we found that the addition of a second chloro substituent at the 2-position of the phenylalanine improved permeability without resulting in a loss of potency, as seen in compound **15** (Tables 4 and 5). Our binding model showed a shallow hydrophobic groove in Cyclin A proximal to the Pro γ-carbon, so we introduced a fluoro substituent at this position in combination with the dichloro-Phe to yield compound **19**, the first submicromolar inhibitor of Cyclin A. Compound **19** also inhibited the Cyclin B **FP2** assay below the limit of quantitation but bound weakly in the Cyclin E **FP2** assay. Conformational assessment of compound **19** suggests that backbone rigidification by incorporation of N-substituted residues helps to further bias the conformational profile toward the putative bound conformation (SI Figure S2). The biochemical potency of **19** translated into antiproliferative activity against NCI-H1048 (0.066 μM) without significant inhibition of WI-38 fibroblast cells, and its permeability was satisfactory (MDCK P_{app} = 1.0 × 10^{-6} cm/s).

Having identified potent, cell-active compound **19**, we were interested in improving the permeability further. In our early scaffold *N*-methylation series, we determined that compound **5** was significantly more permeable than compound **3**, resulting from a single Nε-methylation on the lysine side chain (Table 1). We therefore explored if the cellular potency of **19** would be improved if we (1) reintroduced the lysine side chain methylation identified in compound **5**[41] and (2) increased the size and lipophilicity of the N-terminal capping group (Table 6).[42] Nε-methylation of the lysine side chain resulted in a significant improvement to permeability (**20** and **22**), as expected, but it was also accompanied by a slight decrease in cellular activity in the **19**/**20** matched pair, as well as erosion of selectivity for Cyclin A vs E in each respective matched pair tested in Table 6. Meanwhile, the introduction of the lipophilic cyclohexyl non-fluorinated dipeptide (**21** and **22**), equating to a ∼1 unit increase in AlogP relative to each respective matched pair, afforded only a modest relative increase in permeability and no significant improvements in cell activity. Noting the negative impact of lysine side chain *N*-methylation on the

https://doi.org/10.1021/acs.jmedchem.5c00253
J. Med. Chem. 2025, 68, 17030−17045

Table 6. Improving Permeability of 19 with Lysine Side Chain *N*-Methylation and N-Terminal Residue[a]

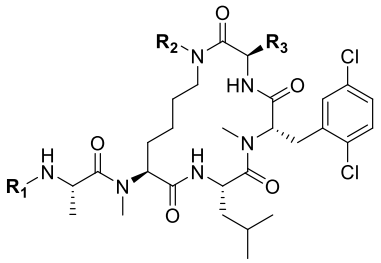

ID	R_1	R_2	R_3	ALogP	CycA FP2 IC_{50} (μM)	CycE FP2 IC_{50} (μM)	H1048 GI_{50} (μM)	WI-38 GI_{50} (μM)	MDCK P_{app} A-B ($x10^{-6}$ cm/s)
19	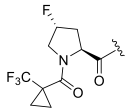	H	$-CH_2CH_2CH_3$	4.1	0.232	2.27	0.066	≥ 20	1
20	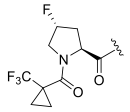	CH_3	$-CH_2CH_2CH_3$	4.4	0.728	1.15	0.369	N/A	12.1
21	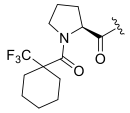	H	$-CH_2CH_3$	4.9	0.044	0.374	≤ 0.152	≥ 20	4.3
22	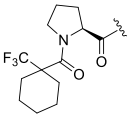	CH_3	$-CH_2CH_3$	5.3	0.039	0.163	≤ 0.147	≥ 13.9	17.4

[a]All compounds in this table have Cyclin B FP $IC_{50} \leq 0.020$ μM; N/A = Not Acquired.

Table 7. Compound 19 Tail Side Chain SAR[a]

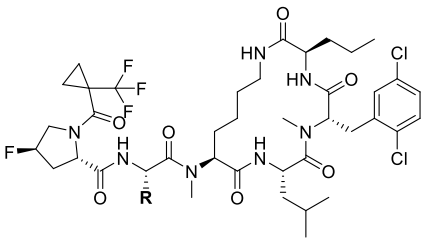

ID	R	ALogP	CycA FP2 IC_{50} (μM)	CycE FP2 IC_{50} (μM)	H1048 GI_{50} (μM)	WI-38 GI_{50} (μM)	MDCK P_{app} A-B ($x10^{-6}$ cm/s)
19	-Me	4.1	0.232	2.270	0.066	≥ 20	1.0
23	-Et	4.5	0.214	0.827	0.105	≥ 10.5	1.6
24	-Pr	4.9	0.439	0.814	0.229	≥ 20	N/A
25	$-CH_2$(cyclobutyl)	5.3	0.632	1.600	0.466	≥ 20	7.0
26	-Cyclopropyl	4.5	0.188	0.729	0.096	N/A	2.3

[a]All compounds in this table have Cyclin B FP $IC_{50} \leq 0.020$ μM; N/A = Not Acquired.

activity of **20**, we redirected our efforts to other regions of the molecule.

Having successfully replaced Arg with neutral residues, we next aimed to determine if further modification of this side chain could improve permeability via modulation of hydrophobicity or potentially improve potency (**R** in Table 7). While increasing the size of the alkyl substituent did improve MDCK permeability, we observed an inverse relationship between the size of the alkyl chain and the biochemical and cellular potency of our compounds (Table 7). Substituting alanine with cyclopropylglycine, seen in compound **26**, provided the optimal balance, providing both activity (biochemical and cellular) and permeability improvements.

We then turned our attention to the residue linking the Lys to the Phe within the macrocycle (**R** in Table 8). Our goal was to retain biochemical activity, cellular potency, and reasonable MDCK permeability while improving kinetic solubility (Ksol) and plasma protein binding (%PPB). Based on our computa-

https://doi.org/10.1021/acs.jmedchem.5c00253
J. Med. Chem. 2025, 68, 17030−17045

Table 8. Compound 26 Macrocycle Core SAR[a]

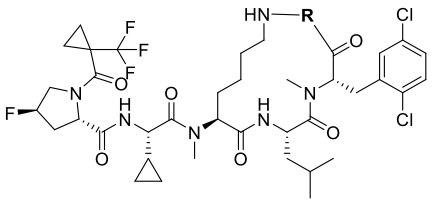

ID	R	ALogP	CycA FP2 IC_{50} (μM)	CycE FP2 IC_{50} (μM)	H1048 GI_{50} (μM)	WI-38 GI_{50} (μM)	MDCK P_{app} A-B (10^{-6} cm/s)	Ksol (μM)	Mouse %PPB
26	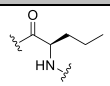	4.5	0.188	0.729	0.096	N/A	2.3	77.3	99.4
27		3.8	0.177	1.84	0.458	14.4	0.3	N/A	N/A
28	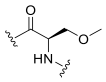	3.3	0.321	0.681	0.196	N/A	0.6	350	N/A
29		4.1	0.262	1.05	0.092	≥ 8.54	0.7	329	93.4
30	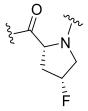	4.1	0.132	0.448	0.176	≥ 12.4	0.3	502	88.8

[a]All compounds in this table have Cyclin B FP $IC_{50} \leq 0.020$ μM; N/A = Not Acquired.

tional binding models, we believed that many residues would be tolerated in place of the existing turn-inducing D-Nva residue. Replacement of the D-Nva in compound **26** with a D-methoxy serine residue in compound **28** improved kinetic solubility, as expected, but the change also resulted in a loss to both biochemical and cellular activity as well as permeability. We were surprised to find that compound **30**, which had a *cis*-D-fluoroproline, did not retain or improve permeability as we had expected due to the elimination of a hydrogen-bond donor, but instead, it showed a substantial decrease in MDCK permeability. It is possible that the backbone amide present in D-Nva and other non-*N*-methylated amino acids could be beneficial to permeability by enabling conformational flexibility and "chameleonicity"[43] via the formation of IMHBs, while the *cis*-D-fluoroproline would introduce structural rigidity and reduce the number of IMHBs. A similar phenomenon in which *N*-alkylation at a chameleonic position led to a decrease in cell permeability was previously observed in *N*-methylated analogues of the cyclic peptide natural product sanguinamide.[44] Also interesting to note is that the kinetic solubility of **30** is significantly higher than that of **26**, further suggesting that the structural rigidity resulting from the incorporation of *cis*-D-fluoroproline could play a larger role in driving physicochemical properties than the number of HBDs in this series.

While compound **27**, containing a cyclopropylglycine residue, showed a 4-fold decrease in cellular activity and significantly lower permeability relative to compound **26**, compound **29**, containing an Aib residue, maintained reasonable biochemical potency and exhibited no loss in cellular activity. The solubility of **29** was substantially improved compared to **26**, concurrent with a decrease in MDCK permeability and %PPB in mice. With this promising balance of activity and in vitro PK parameters, we moved on to the final stages of optimization.

Selection of 34 for the First PoC Efficacy Study. We focused on the following selection criteria to nominate the compound for our proof-of-concept efficacy study. First, we started from the assumption that achieving plasma-free drug concentrations that met or exceeded the in vitro GI_{50} value would be minimally required for in vivo efficacy, thus highlighting the importance of cellular potency and in vivo exposure for compound selection.[45,46] Second, as the activity of this class of agents relies on inhibiting Cyclins that are expressed transiently during certain phases of the cell cycle, and as cells within tumors are not synchronized, we assumed daily dosing and some time frame of exposure per day would correlate with the best effect as opposed to intermittent dosing. Third, to minimize the potential for toxicity in vivo, we required >100-fold selective activity toward the target cell lines versus the WI-38 nontransformed fibroblast cell line. Also, based on our observations that dual Cyclin A/B RxL inhibition is required for optimal synthetic lethality in E2F-driven cancer cells and that Cyclin E activity is dispensable, we desired selectivity for Cyclin A/B over E inhibition of >10-fold in a lead selected for in vivo testing.[28] Finally, to set the stage for future improvements in oral bioavailability, we preferred to select a lead compound with good cell permeability and relatively low levels of efflux liability. With these criteria and the prior SAR in mind, we set about altering the fluorinated lipophilic tail terminus as the final region where optimization might deliver compounds with the desired characteristics. Compound **29** in Table 8 was selected as a starting point for the final round of SAR, as it was among the most potent

https://doi.org/10.1021/acs.jmedchem.5c00253
J. Med. Chem. 2025, 68, 17030−17045

Table 9. N-Terminal Cap Optimization to Balance Properties[a]

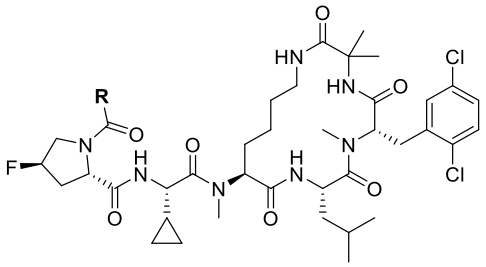

ID	R	ALogP	CycA FP2 IC_{50} (μM)	CycE FP2 IC_{50} (μM)	H1048 GI_{50} (μM)	WI-38 GI_{50} (μM)	MDCK P_{app} A-B ($x10^{-6}$ cm/s)	CACO-2 A-B ($x10^{-6}$ cm/s)	CACO-2 B-A ($x10^{-6}$ cm/s)	ER (B-A/A-B)	Ksol (μM)	Mouse %PPB
29	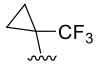	4.1	0.262	1.050	0.092	≥ 8.54	0.7	0.1	5.54	55	329	93.4
31	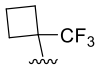	4.5	0.053	0.242	0.025	≥ 19.8	0.7	0.08	6.95	87	139	96.9
32	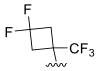	4.7	0.034	0.470	≤ 0.091	≥ 13.2	0.9	Below LOQ	8.88	N/A	109	96.7
33	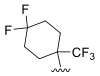	5.5	0.020	0.142	≤ 0.011	9.35	0.8	0.07	4.50	64	12.2	98.1
34		5.3	0.079	0.958	0.042	≥ 8.41	3.6	0.36	8.02	22	18.9	97.3

[a]All compounds in this table have Cyclin B FP $IC_{50} \leq 0.020$ μM; N/A = Not Acquired.

against the NCI-H1048 cell line and had excellent kinetic solubility, but was lacking in selectivity, permeability, and had a high efflux liability (Table 9). Expanding the tail terminal ring to a cyclobutyl in compound **31** improved both biochemical and cellular potency but without improving other parameters. Difluorination of the cyclobutyl group in compound **32** delivered an improvement of selectivity to 14-fold for Cyclin A vs Cyclin E without improving permeability or efflux. Our models predict this group projects into solvent, so the structural basis for the increase in selectivity is not obvious. Expansion of the cycloalkyl group to a difluorocyclohexyl in compound **33** improved cellular potency but at the cost of selectivity, consistent with results in Table 6. Finally, the spiro-bis-cyclobutyl moiety in compound **34** delivered the desired improvements in cellular potency, selectivity, and permeability, along with a reduced efflux liability (Figure 4). We selected a second Rb-dysregulated cell line with high baseline E2F activity, the NCI-H69 SCLC line, as an additional model to provide further confirmation of efficacy. Compound **34** was found to be approximately 3-fold more potent against the NCI-H69 cell line than the NCI-H1048 cell line, as its in vitro GI_{50} was 0.016 μM vs NCI-H69 compared to 0.048 μM vs NCI-H1048 (Table 9). Compound **34** was advanced into mouse studies to determine its PK parameters via multiple routes of administration. As seen in Table 10, compound **34** demonstrated a relatively modest 2.2% oral bioavailability; thus, the exposure via oral dosing was too limited for use in a POC study. However, intraperiotoneal (IP) dosing at 100 mg/kg of **34** resulted in free plasma Cmax values that exceeded the in vitro GI_{50} value for the NCI-H1048 and NCI-H69 cell lines as desired.

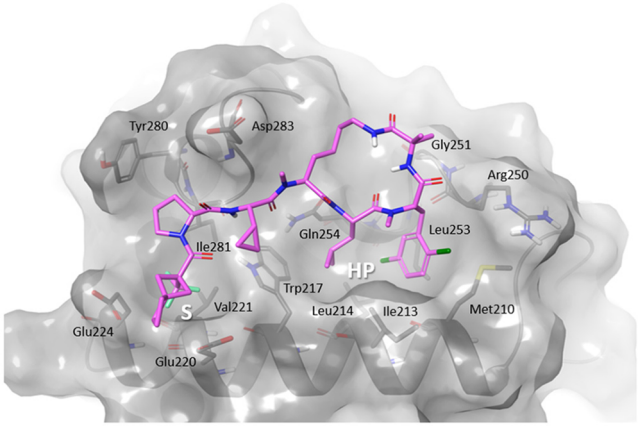

Figure 4. Model of compound **34** bound to Cyclin A. The 2,5-dichloro-phenylalanine and the N-terminal trifluoromethane improved contacts at the HP and S pockets, respectively. The hydrogen bonding network at the binding interface was expected to be preserved as backbone N-substitutions were limited to solvent-exposed amides.

In Vivo Proof-of-Concept with a First in Class Cyclin A/B RxL Inhibitor in SCLC Tumor Xenograft Mouse Models. We evaluated the in vivo antitumor activity of compound **34** in two SCLC cell line-derived xenograft (CDX) models, NCI-H1048 and NCI-H69 (Figures 5 and S4). Compound **34** was tested first in the NCI-H1048 model, dosed at 50 and 100 mg/kg intraperitoneally (IP) once daily (QD) for 14 days. Treatment with compound **34** induced substantial tumor growth inhibition (TGI) in the NCI-H1048 model, with a mean % tumor growth inhibition (%TGI) value

https://doi.org/10.1021/acs.jmedchem.5c00253
J. Med. Chem. 2025, 68, 17030−17045

Table 10. Mouse IV, PO, and IP PK Parameters of Compound 34

Route of administration	Dose (mg/kg)	T_{max} (h)	C_{max} (total drug; ng/mL)	C_{max} (free drug; nM)	AUC0-inf (ng*h/mL)	$T_{1/2}$ (h)	Cl (mL*min/kg)	%F
IV	2	-	-	-	919	0.99	36.3	-
PO	30	1.0	13	0.36	39.4	1.26	-	2.2
IP	100	2	3,720	103	20,400	7.14	-	-

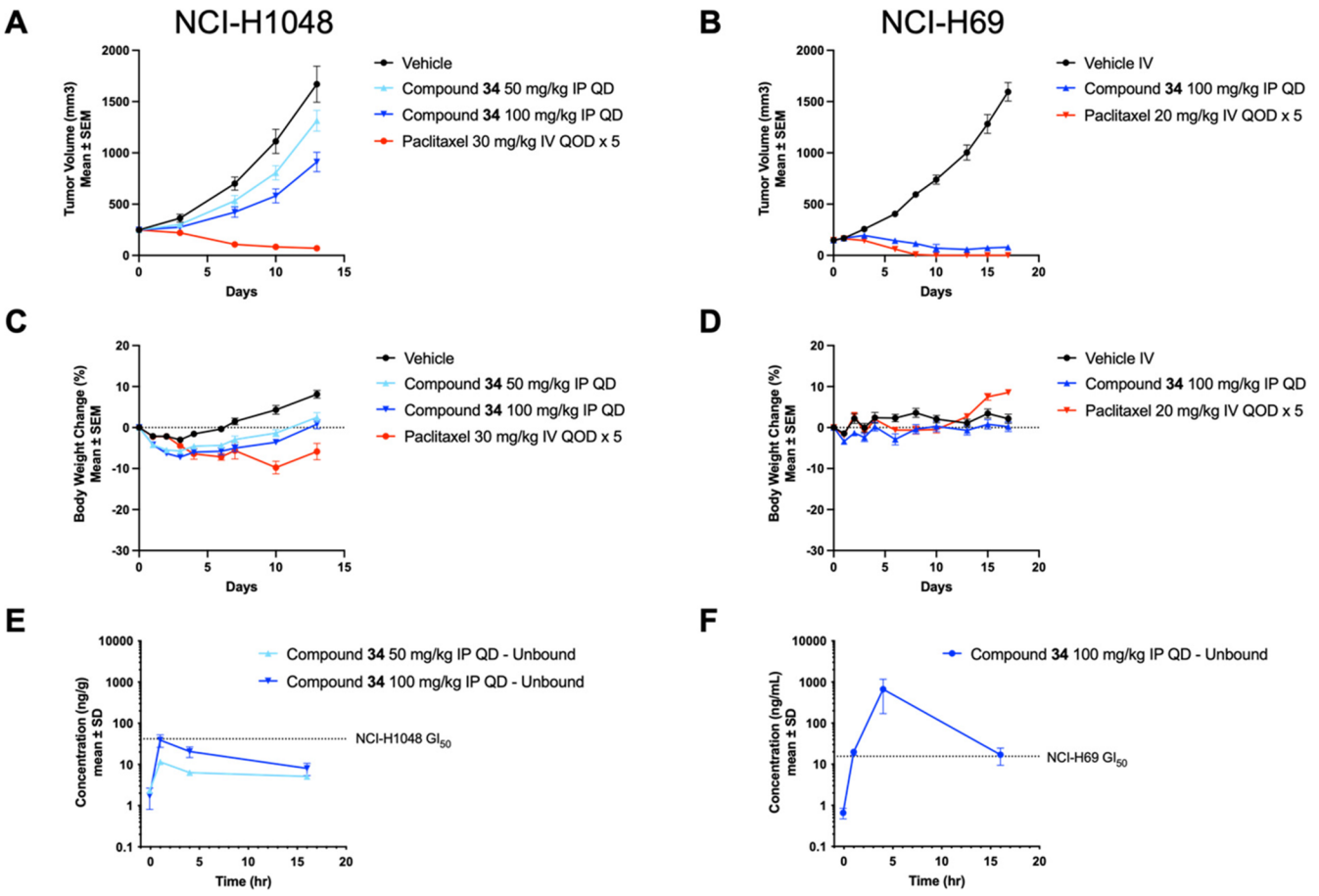

Figure 5. Cyclin A/B RxL inhibitor has antitumor activity in the NCI-H1048 and NCI-H69 SCLC xenograft models. (A) Tumor volume curves for NCI-H1048 xenograft tumors treated with vehicle or compound **34** at 50 and 100 mg/kg IP QD for 14 days or paclitaxel at 30 mg/kg IV every other day (QOD) × 5 (9 days). (B) Tumor volume curves for NCI-H69 xenograft tumors treated with vehicle or compound **34** at 100 mg/kg IP QD for 18 days or paclitaxel at 20 mg/kg IV QOD × 5 (9 days). (C, D) Body weight change for treated animals. (E, F) Unbound plasma concentration of compound **34** in animals after the final dose. For (A–E), n = 10 mice per arm. For (F), n = 3–10 mice per time point. For (A–D), Data are mean ± SEM. For (E, F), data are mean ± 1 SD.

of 53% at the 100 mg/kg dose level. A dose–response was seen between the 50 and 100 mg/kg groups.

Following this, compound **34** was tested in the NCI-H69 model at 100 mg/kg QD. The antitumor effect of compound **34** treatment was more striking in the NCI-H69 model, inducing a mean %TGI value of 105% with 60% complete regressions (CR) and 40% tumor-free survival. Plasma PK analysis revealed that unbound drug exposure relative to GI_{50} was more substantial in the NCI-H69 study, correlating with the increased antitumor activity in that model. In both models, treatment with compound **34** was well tolerated, with mean body weight loss not exceeding 10% over the course of the studies. These results confirm that macrocyclic Cyclin A/B RxL inhibitors may present a new treatment option for patients with SCLC.

In Vitro Evaluation of Potential Off-Target Toxicity with 34. Beyond the observed tolerability in mouse PK and efficacy studies, the question of the potential safety of this new class of anticancer agents is important to consider. Macrocyclic peptides have been touted as a drug class that combines the benefits of large biomolecules, including high potency and exquisite selectivity, with those of small molecules, including reasonable manufacturing costs, favorable pharmacokinetic properties, ease of administration, lack of immunogenicity, and generally have excellent safety profiles.[47]

Evaluation of compound **34** in a panel of 489 kinases at 1 and 10 μM test concentrations showed a clean profile, as

https://doi.org/10.1021/acs.jmedchem.5c00253
J. Med. Chem. 2025, 68, 17030–17045

expected, given the mechanism of action of this novel class of agents (SI Table S5). Compound **34** also demonstrated no significant off-target activity when tested at 10 μM in a safety pharmacology functional panel that included 6 voltage and ligand-gated ion channels, 24 cell-based assays to evaluate both agonistic and antagonistic activity, and 10 enzyme inhibition assays (SI Tables S6–S17). Finally, compound **34** demonstrated moderate to low levels of inhibition of human cytochrome P450 enzymes in vitro, indicating a moderate to low potential for drug–drug interactions mediated via Cyp inhibition (SI Tables S18 and S19).

CONCLUSIONS

Herein, we report the discovery of a novel class of Cyclin A/B RxL inhibitors displaying potent and selective antiproliferative activity against SCLC tumor cells and modest oral bioavailability. We further demonstrate promising antitumor activity with a lead compound from this series in SCLC mouse tumor models. This marks the first time, despite decades of interest in these "undruggable" targets, that a compound series targeting the Cyclin A hydrophobic patch has advanced to this stage and demonstrated its potential as a source for a new class of anticancer agents. This was accomplished using a permeability-first design approach in which we focused first on identifying cell-permeable scaffolds and subsequently utilized a combination of computationally guided structure-based design and solid-phase synthesis to incorporate features to drive potency and selectivity. Our findings not only provide a proof-of-concept that Cyclin A/B are viable oncology targets but also demonstrate the utility of macrocyclic modalities for modulating previously undruggable intracellular targets. The work reported here continued to deliver a clinical candidate, which will be disclosed in future publications.[26]

EXPERIMENTAL SECTION

Synthesis and Characterization. Unless otherwise mentioned, all solvents and chemicals were obtained from commercial sources and used without purification. Linear sequences were synthesized in parallel on a Biotage Syro II peptide synthesizer equipped with 48 reaction vials using 2-chlorotrityl chloride resin, Fmoc-protected amino acids, and hexafluorophosphate azabenzotriazole tetramethyl uronium (HATU) coupling. Site-specific on-resin methylation was achieved using a modified Fukuyama-Mitsunobu protocol in toluene on the same instrument.[30] Linear peptides were cleaved from the resin with trifluoroacetic acid (TFA) or hexafluoro-2-propanol (HFIP), concentrated under reduced pressure, and cyclized using propanephosphonic acid anhydride (T3P) or PyBop with diisopropylethylamine (DIEA) in dichloromethane (DCM)/dimethylformamide (DMF). All cyclized products were then purified via HPLC, yielding 1–10 mg of material of >95% purity by HPLC. The progress of reactions was typically monitored by LCMS (Waters UPLC Acquity I-Class equipped with Acquity QDa). Purification of final compounds to >95% purity was carried out by reverse phase C18 chromatography using a Waters HPLC system equipped with the following components: Waters 2767 Sample Manager, Waters 1525 Binary HPLC Pump, Waters 2545 Binary Gradient Module, Waters SFO System Fluidics Organizer, 515 HPLC Pump, Waters Acquity QDA, and Waters 2998 Photodiode Array Detector. Proton (1H) and carbon (13C) NMR spectra were recorded on a Bruker Avance 500 (500.13 MHz for 1H; 125.76 MHz for 13C) using DMSO-d_6 as a solvent. Chemical shifts are given in parts per million (ppm) (δ relative to residual solvent peak for 1H and 13C).

Computational Model and Binding Affinity Predictions. Models of compounds bound to Cyclin A were generated by the previously reported method.[28] The docking study reported in Table 2 was carried out with Schrodinger suite 2020-4. The initial compound structures were generated using a model template constructed from Cyclin A-bound cocrystallized ligands, including the p27kip2 peptide (PDB: 1JSU) and a lariat macrocycle (PDB: 1URC). The input compound structures were refined in the RxL binding site by running Glide SP docking with the "refine-only" option, followed by MM-GBSA postscoring using Prime with the rigid protein model. The ligand interaction diagram in Figure 2 was generated using Maestro.

Calculated and Measured Compound Properties. AlogP and PSA values were calculated by using the Quick Properties model in LiveDesign. Membrane insertion free energies, ΔG_{insert}, were calculated using the Physics-Based Membrane Permeability module in Schrodinger Suite 2023-3 with default settings and conformational sampling. The input compound structures were prepared by using the LigPrep module prior to the permeability calculation. MDCK monolayer cell permeability, kinetic solubility (Ksol), mouse plasma protein binding via ultracentrifugation (%PPB), and Caco-2 monolayer permeability (A–B and B–A) were generated by Quintara Discovery Inc. using standard experimental conditions (see the SI in vitro assay experimental methods for details).

Cell Lines and Cell Culture. NCI-H1048, NCI-H69, and WI-38 cell lines were originally obtained from the American Type Culture Collection (ATCC). NCI-H69 cells were maintained in RPMI-1640 media supplemented with 10% fetal bovine serum (FBS), NCI-H1048 cells were maintained in HITES medium (Base medium: DMEM:F12 supplemented with 0.001 mg/mL insulin, 0.01 mg/mL Transferrin, 30 nM selenium, 10 nM hydrocortisone, 10 nM β-estradiol, and additional 2 mM glutamine to a final concentration of 4.5 mM) supplemented with 5% fetal bovine serum (FBS). WI-38 cells were maintained in DMEM supplemented with 10% FBS.

Early passage cells of all of the cell lines listed above were frozen using Recovery Cell Culture Freezing media (Gibco) and were maintained in culture for no more than 4 months, where early passage vials were thawed.

MTT Proliferation Assay. NCI-H1048 and WI-38 cell lines were plated in 96-well plates at 5×10^3 cells/well with 100 mL of media/well. NCI-H69 cells were grown to confluency in a T150 flask. Cells were collected by centrifugation at 1100 rpm and resuspended in 30 mL media, of which 10 mL was used to seed six 96-well plates. The following day, cells were dosed using a Bravo liquid Handler (Agilent Technologies). The plate controls Roscovitine and Staurosporine were used to define the top and bottom of the growth inhibition curves, respectively. Inhibitors were dosed in duplicate in either an 8- (WI-38, NCI-H1048) or 10-point (NCI-H69) 1:3 serial dilution with 10 μM maximum concentration. Roscovitine was dosed in a singlet in an 8- or 10-point 1:2 serial dilution with a 100 μM maximum concentration. Staurosporine was dosed in a singlet in an 8- or 10-point 1:2 serial dilution with 1 μM maximum concentration. After dosing, plates were maintained in tissue culture incubators (37 °C; 5% CO_2) for 3 (WI-38) or 5 days (NCI-H1048, NCI-H69) to allow for at least 2 cell doublings before processing in an MTT proliferation assay (R&D systems, #4890-050-K) performed according to manufacturer instructions. The average absorbance value obtained with the highest two concentrations dosed for roscovitine and staurosporine was used for background subtraction. The top of the assay (100% growth) was determined by normalization with the top of the roscovitine curve. Growth inhibition 50 (GI_{50}) was determined by nonlinear regression analysis using log(inhibitor) vs response–variable slope (four parameters) using GraphPad Prism (10.1.0) software.

Fluorescence Polarization Assay. Binding affinity for the compounds of Formula I was determined by the Fluorescence Polarization (FP) competitive assay based on previously established protocols[14,27] with modifications as described below. Cyclin/CDK protein complexes were sourced as follows: Cyclin A2/CDK2 (CRELUX Protein Services), Cyclin B1/CDK1 (Eurofins, discovery. Cat. No. 14-450), and Cyclin E1/CDK2 (Eurofins, discovery. Cat. No. 14-475). FP binding assays were performed in 25 mM HEPES (pH 7.5), 100 mM NaCl, 1 mM DTT, 0.01% NP-40, and 1 mg/mL BSA for all 3 protein complexes in black 96-well plates. After experimental plates were set, they were equilibrated by gentle mixing

https://doi.org/10.1021/acs.jmedchem.5c00253
J. Med. Chem. 2025, 68, 17030–17045

by placing them on an orbital shaker at 100 rpm for 2 h at rt and then read on a SpectraMax i3X Multi-Mode Microplate Detection platform. The affinity of the Cyclin/CDK complexed for the fluorescently labeled probe was determined by adding increasing concentration of each protein complex in a buffer containing a carboxyfluorescein labeled probe (5-carboxyfluorescein (FAM) probe) at 2 nM (preparation of the FAM probe is described below). In the first-generation assay (**FP1**) using the "**FP1** probe" (Supporting Information), the concentration of Cyclin A/Cdk2 was 20 nM, while in the second-generation assay (**FP2**) using the "**FP2** probe" (Supporting Information), we used 8 nM for Cyclin A2/CDK2, and 10 nM for both Cyclin B1/CDK1 and Cyclin E1/CDK2. Methods to prepare the FAM probes are described in the heading below. Under these conditions, the dynamic range was >100 mP between 100% binding of FAM probe and complete inhibition of binding by saturating excess of an unlabeled competitor compound, with all experiments showing a Z' factor >0.80. IC_{50} values for test compounds were determined in eight-point serial dilution dose−response curves. Reported IC_{50} values are the average of 2−3 independent experiments.

Preclinical Pharmacokinetics Studies. All experiments were performed following the guidance of the Association for the Assessment and Accreditation of Laboratory Animal Care (AAALAC). All procedures were approved by the Institutional Animal Care and Use Committee of the testing facilities.

Single Dose Intravenous (IV) and Oral (PO) PK in Mice. Compound **34** was dissolved in 5% DMSO:10% Solutol HS15:85% DI water to yield a concentration of 0.4 mg/mL for the IV formulation and prepared in 5% DMSO: 50% PEG400:45% D5W 1.0 mg/mL to yield a concentration of 3.0 mg/mL for the PO formulation. N = 3 mice each were dosed at 3 mg/kg via tail vein (IV) and 30 mg/kg via oral gavage (PO). Approximately 0.05 mL of blood was collected from a tail or facial vein in tubes containing K3 EDTA at 0.083, 0.25, 0.5, 1, 3, and 8 h post-IV and post-PO dose. Plasma samples were obtained via centrifugation, and sample cleanup was conducted by protein precipitation with acetonitrile that contained an internal standard (IS, Arachidonoyl Ethanolamide-d_4). LCMS/MS (AB Sciex 6500 and Acquity UPLC) quantitation of **34** and IS was achieved with positive ion MRM transitions of 972.8/570.2. The reversed-phase chromatographic system consisted of a gradient mobile phase at a flow rate of 0.8 mL/min, containing 0.1% formic acid in water and acetonitrile and a Waters BEH C18 2.1 × 50 mm. Analyst version 1.6.2 was used to measure peak areas and peak area ratios of **34** to IS. A calibration curve was constructed from the peak area ratios (Compound **34** to IS) with a weighted (1/×2) linear regression using Watson version 7.5 LIMS and a calibration curve ranging between 2.0 and 10,000 ng/mL. Individual compound **34** plasma concentration vs time profiles were used to calculate the pharmacokinetic parameters by employing a noncompartmental analysis (Phoenix WinNonlin 8.3).

Single Dose Intraperitoneal (IP) PK in Mice. Compound **34** was dissolved in DMSO: Solutol HS15: D5W (5:10:85, v/v/v) to yield a concentration of 10 mg/mL for the IP dose at 100 mg/kg. One dose group of N = 3 mice each were dosed at 100 mg/kg in single dose IP dosing. Approximately 0.05 mL of blood was collected from a tail or facial vein in tubes containing K3 EDTA at 0.083, 0.25, 0.5, 1, 2, 4, 8, 24, and 48 h post-IP dose. Plasma samples were obtained via centrifugation, and sample cleanup was conducted by protein precipitation with acetonitrile that contained an internal standard (IS, Warfarin). LCMS/MS (AB Sciex 5000 and Shimadzu LC-30AD) quantitation of **34** and IS was achieved with positive ion MRM transitions of 972.8/439.3. The reversed-phase chromatographic system consisted of a gradient mobile phase at a flow rate of 0.65 mL/min, containing 0.1% formic acid in water and acetonitrile and an ACE 5 C8, 2.1 mm × 50 mm, 5 μm. Analyst version 1.6.2 was used to measure peak areas and peak area ratios of compound **34** to IS. A calibration curve was constructed from the peak area ratios (**34** to IS) with a weighted (1/×2) linear regression using Watson version 7.5 LIMS and a calibration curve ranging between 1.0 and 5000 ng/mL. Individual compound **34** plasma concentration vs time profiles were used to calculate the pharmacokinetic parameters by employing a noncompartmental analysis (Phoenix WinNonlin 8.3).

SCLC Cell Line Xenograft Studies. All experiments conducted were performed following the guidance of the Association for Assessment and Accreditation of Laboratory Animal Care (AAALAC). The NCI-H1048 xenograft study was approved by the Institutional Animal Care and Use Committee (IACUC) and performed at Pharmaron (Ningbo) Technology Development Co. Ltd. (Animal Use Protocol Number: ON-CELL-XEN-06012021). The NCI-H69 xenograft study was approved by the IACUC and performed at Labcorp Early Development Laboratories, Inc. (Animal Use Protocol Number: VUF 05).

NCI-H1048 and NCI-H69 human small-cell lung cancer cells were obtained from ATCC. Tumor volume was determined by measuring the length (L) and perpendicular width (W) with calipers and calculated using the formula $0.5 \times L \times W^2$.

As a measure of efficacy, the % tumor growth inhibition (%TGI) is calculated at the end of the experiment using the following formula

$$\text{mean \%TGI} = 100 - \left(\left(\frac{\Delta T_{\text{mean}}}{\Delta C_{\text{mean}}}\right) \times 100\right)$$

ΔT_{mean} and ΔC_{mean} represent the mean volume on the day of evaluation minus the tumor volume at the start of dosing for the treatment and control groups, respectively. Tumors that have a smaller volume at the end of the study in comparison to the volume at the start of dosing will have %TGI values greater than 100%.

For the NCI-H1048 model, 3×10^6 NCI-H1048 cells were suspended in a 1:1 mixture of HITES media and Matrigel (Corning no. 354234) and implanted subcutaneously into the flanks of 6−8 week old female BALB/c nude mice (GemPharmatech Biotech Co., Ltd., #D000521). When tumors were 160−370 mm^3 in size, 18 days after implantation, mice were randomized and put into treatment groups of compound **34**, paclitaxel (Beijing Shuanglu no. 20210202), or vehicle (5% DMSO, 10% Solutol HS15, in 85% water). Mice were treated daily with intraperitoneal (IP) injections of 50 or 100 mg/kg compound **34** or vehicle for 14 days or with IV injections of 30 mg/kg paclitaxel every other day for 5 doses. Tumors were measured twice per week for the duration of the study, while body weight was measured daily for 5 days and then twice per week for the duration of the study. Plasma samples were collected for PK analysis by LCMS/MS at multiple time points shown on day 14.

For the NCI-H69 model, 5×10^6 NCI-H69 cells were suspended in serum-free RPMI-1640 media, combined with an equal volume of ECM gel (Sigma-Aldrich #E1270), and implanted subcutaneously into the flanks of 7−8 week old female Nude mice (Envigo, Hsd:Athymic Nude-*Foxn1*^{nu}). When tumors were 100−200 mm^3 in size, 13 days after implantation, the mice were randomized and put into treatment groups. Mice were treated daily with IP injections of 100 mg/kg compound **34** or vehicle (5% DMSO, 10% Solutol HS15, in 85% D5W) for 18 days or with IV Injections of 20 mg/kg paclitaxel every other day for 5 doses. Tumors were measured three times per week for the duration of the study, while body weight was measured daily for 5 days and then three times per week for the duration of the study. Plasma samples were collected for PK analysis by LCMS/MS at multiple time points shown on day 18.

In Vitro Safety and Metabolism Testing. Eurofins Discovery Services carried out the in vitro safety testing of compound **34**. The tests selected were from the Eurofins product list and included (i) The KINOMEscan kinase panel assay set containing 468 kinases; (ii) the SAFETYScreen 47 predominantly cell-based Functional Panel that includes 24 pharmacology targets tested against for both agonist and antagonist activities, 10 enzymes and transporters tested for antagonist activities, and an Ion-Profiler panel containing 6 voltage and ligand-gated ion channels; and (iii) the ADME-Tox In Vitro Metabolism Inhibition panel of 7 major human cytochrome P450 enzymes. In each case, compound **34** was tested at either a single concentration or at two test concentrations.

https://doi.org/10.1021/acs.jmedchem.5c00253
J. Med. Chem. 2025, 68, 17030−17045

■ ASSOCIATED CONTENT

Supporting Information

The Supporting Information is available free of charge at https://pubs.acs.org/doi/10.1021/acs.jmedchem.5c00253.

Solid-phase peptide synthesis methods; purification and analytical methods; building blocks and peptide sequences; analytical data, SMILES strings; computational methods and conformational profiling data; synthetic schemes and experimental details for building blocks, compound **34**, and FP probes; spectral data: NMR for custom building blocks, LCMS for FP probes, and both NMR and LCMS/HPLC traces for compound **34**; Eurofins KINOMEscan Profiling and SafetyScreen details for compound **34**; in vitro assay methods for MDCK, Caco-2, plasma protein binding, and kinetic solubility (PDF)

SMILES of macrocyclic inhibitors (CSV)

Binding model of **7** with Cyclin A (PDB)

Binding model of **34** with Cyclin A (PDB)

■ AUTHOR INFORMATION

Corresponding Author

James B. Aggen − *Circle Pharma, Inc., South San Francisco, California 94080, United States;* orcid.org/0000-0001-7989-5131; Email: jim.aggen@circlepharma.com

Authors

Andrew T. Bockus − *Circle Pharma, Inc., South San Francisco, California 94080, United States;* orcid.org/0000-0001-5522-6523

Siegfried S. F. Leung − *Circle Pharma, Inc., South San Francisco, California 94080, United States*

Breena Fraga-Walton − *Circle Pharma, Inc., South San Francisco, California 94080, United States*

Miguel P. Baldomero − *Circle Pharma, Inc., South San Francisco, California 94080, United States*

Luis Hernandez − *Circle Pharma, Inc., South San Francisco, California 94080, United States*

Nathan J. Dupper − *Circle Pharma, Inc., South San Francisco, California 94080, United States*

Justin A. Shapiro − *Circle Pharma, Inc., South San Francisco, California 94080, United States;* orcid.org/0000-0001-9891-0464

Bryan M. Lent − *Circle Pharma, Inc., South San Francisco, California 94080, United States*

David C. Spellmeyer − *Circle Pharma, Inc., South San Francisco, California 94080, United States*

Megan K. DeMart − *Circle Pharma, Inc., South San Francisco, California 94080, United States*

Joshua Luna − *Circle Pharma, Inc., South San Francisco, California 94080, United States*

Dalena Hoang − *Circle Pharma, Inc., South San Francisco, California 94080, United States*

Manesh Chand − *Circle Pharma, Inc., South San Francisco, California 94080, United States;* Present Address: University of California, Davis, Davis, California 95616, United States

Yuliana Gritsenko − *Circle Pharma, Inc., South San Francisco, California 94080, United States;* Present Address: New Culture, Inc., San Leandro, California 94577, United States

Cayla McEwen − *Circle Pharma, Inc., South San Francisco, California 94080, United States;* Present Address: Sangamo Therapeutics, Richmond, California 94804, United States

Mahesh Ramaseshan − *Circle Pharma, Inc., South San Francisco, California 94080, United States;* Present Address: Stoke Therapeutics, Bedford, Massachusetts 01730, United States

Catherine E. Gleason − *Circle Pharma, Inc., South San Francisco, California 94080, United States*

Frances Hamkins-Indik − *Circle Pharma, Inc., South San Francisco, California 94080, United States*

Miles W. Membreno − *Circle Pharma, Inc., South San Francisco, California 94080, United States;* Present Address: University of California, Santa Cruz, California 95064, United States

Jie Zheng − *Circle Pharma, Inc., South San Francisco, California 94080, United States;* Present Address: Olema Oncology, San Francisco, California 94103, United States

Ranya Odeh − *Circle Pharma, Inc., South San Francisco, California 94080, United States*

Meisam Nosrati − *Circle Pharma, Inc., South San Francisco, California 94080, United States*

Daphne He − *Circle Pharma, Inc., South San Francisco, California 94080, United States*

Ramesh Bambal − *Circle Pharma, Inc., South San Francisco, California 94080, United States;* Present Address: Prelude Therapeutics, Wilmington, Delaware 19805, United States

Peadar Cremin − *Circle Pharma, Inc., South San Francisco, California 94080, United States*

Jinshu Fang − *Circle Pharma, Inc., South San Francisco, California 94080, United States*

Bernard Levin − *Circle Pharma, Inc., South San Francisco, California 94080, United States*

Evelyn W. Wang − *Circle Pharma, Inc., South San Francisco, California 94080, United States;* Present Address: Evelyn Wang Consulting, San Francisco, California 94114, United States

Marie Evangelista − *Circle Pharma, Inc., South San Francisco, California 94080, United States*

David Earp − *Circle Pharma, Inc., South San Francisco, California 94080, United States*

Constantine Kreatsoulas − *Circle Pharma, Inc., South San Francisco, California 94080, United States*

Rajinder Singh − *Circle Pharma, Inc., South San Francisco, California 94080, United States;* Present Address: Stealth Biotech, San Carlos, California, United States

Pablo D. Garcia − *Circle Pharma, Inc., South San Francisco, California 94080, United States*

Complete contact information is available at: https://pubs.acs.org/10.1021/acs.jmedchem.5c00253

Author Contributions

‡A.T.B. and S.S.F.L. contributed equally. This manuscript was written through contributions of all authors. All authors have given approval to the final version of the manuscript.

Notes

All work described herein was performed by authors while employed by Circle Pharma, Inc.

The authors declare no competing financial interest.

■ ACKNOWLEDGMENTS

The authors thank Matthew P. Jacobson, William G. Kaelin Jr., Alan Ashworth, Bruce Stillman, John Josey, George Tonn, Steve Olson, and Ronald Zuckermann for their support and insightful discussions.

■ ABBREVIATIONS USED

bRo5, beyond rule-of-five; CDK, cyclin-dependent kinase; CDX, cell line-derived xenograft; CR, complete regression; DCM, dichloromethane; DIEA, diisopropylethylamine; DMF, dimethylformamide; E2F, early region 2 binding factor; FAM, 5-carboxyfluorescein; FP, fluorescence polarization assay; HATU, hexafluorophosphate azabenzotriazole tetramethyl uronium; HBA, hydrogen-bond acceptor; HBD, hydrogen-bond donor; HFIP, hexafluoro-2-propanol; HP, hydrophobic patch; IMHB, intramolecular hydrogen bond; IP, intraperiotoneal; LOQ, limit of quantitation; MDCK, Madin-Darby canine kidney cells; MM-GBSA, molecular mechanics generalized Born surface area; MRAIL, domain composed of methionine, arginine, alanine, isoleucine, leucine in cyclins; P_{app}, apparent permeability; PO, "per os" oral dosing; PPB, plasma protein binding; PPI, protein−protein interaction; QD, once daily dosing; QOD, every other day dosing; RB/RB1, retinoblastoma protein; RxL, motif composed of arginine, a variable moiety, and leucine; SAR, structure activity relationship; SCLC, small cell lung cancer; T3P, propanephosphonic acid anhydride; TAT, trans-activator of transcription; TFA, trifluoroacetic acid; TGI, tumor growth inhibition; TPSA, total polar surface area

■ REFERENCES

(1) Morgan, D. O. *The Cell Cycle: Principles of Control*, 1st ed.; Sinauer Associates Inc, 2006.
(2) Otto, T.; Sicinski, P. Cell Cycle Proteins as Promising Targets in Cancer Therapy. *Nat. Rev. Cancer* **2017**, *17* (2), 93−115.
(3) Suski, J. M.; Braun, M.; Strmiska, V.; Sicinski, P. Targeting Cell-Cycle Machinery in Cancer. *Cancer Cell* **2021**, *39* (6), 759−778.
(4) Arter, C.; Trask, L.; Ward, S.; Yeoh, S.; Bayliss, R. Structural Features of the Protein Kinase Domain and Targeted Binding by Small-Molecule Inhibitors. *J. Biol. Chem.* **2022**, *298* (8), No. 102247.
(5) Lipinski, C. A.; Lombardo, F.; Dominy, B. W.; Feeney, P. J. Experimental and Computational Approaches to Estimate Solubility and Permeability in Drug Discovery and Development Settings. *Adv. Drug Delivery Rev.* **1997**, *23* (1−3), 3−25.
(6) Wang, X.; Zhao, S.; Xin, Q.; Zhang, Y.; Wang, K.; Li, M. Recent Progress of CDK4/6 Inhibitors' Current Practice in Breast Cancer. *Cancer Gene Ther.* **2024**, *31* (9), 1283−1291.
(7) Álvarez-Fernández, M.; Malumbres, M. Mechanisms of Sensitivity and Resistance to CDK4/6 Inhibition. *Cancer Cell* **2020**, *37* (4), 514−529.
(8) Łukasik, P.; Baranowska-Bosiacka, I.; Kulczycka, K.; Gutowska, I. Inhibitors of Cyclin-Dependent Kinases: Types and Their Mechanism of Action. *Int. J. Mol. Sci.* **2021**, *22* (6), 2806.
(9) Adams, P. D.; Sellers, W. R.; Sharma, S. K.; Wu, A. D.; Nalin, C. M.; Kaelin, W. G. Identification of a Cyclin-Cdk2 Recognition Motif Present in Substrates and P21-like Cyclin-Dependent Kinase Inhibitors. *Mol. Cell. Biol.* **1996**, *16* (12), 6623−6633.
(10) Schulman, B. A.; Lindstrom, D. L.; Harlow, E. Substrate Recruitment to Cyclin-Dependent Kinase 2 by a Multipurpose Docking Site on Cyclin A. *Proc. Natl. Acad. Sci. U.S.A.* **1998**, *95* (18), 10453−10458.
(11) Russo, A. A.; Jeffrey, P. D.; Patten, A. K.; Massagué, J.; Pavletich, N. P. Crystal Structure of the p27Kip1 Cyclin-Dependent-Kinase Inibitor Bound to the Cyclin A−Cdk2 Complex. *Nature* **1996**, *382* (6589), 325−331.
(12) Klein, M. Targeting Protein-Protein Interactions to Inhibit Cyclin-Dependent Kinases. *Pharmaceuticals* **2023**, *16* (4), 519.
(13) Chen, Y.-N. P.; Sharma, S. K.; Ramsey, T. M.; Jiang, L.; Martin, M. S.; Baker, K.; Adams, P. D.; Bair, K. W.; Kaelin, W. G. Selective Killing of Transformed Cells by Cyclin/Cyclin-Dependent Kinase 2 Antagonists. *Proc. Natl. Acad. Sci. U.S.A.* **1999**, *96* (8), 4325−4329.
(14) Premnath, P. N.; Craig, S. N.; Liu, S.; Anderson, E. L.; Grigoroudis, A. I.; Kontopidis, G.; Perkins, T. L.; Wyatt, M. D.; Pittman, D. L.; McInnes, C. Iterative Conversion of Cyclin Binding Groove Peptides into Druglike CDK Inhibitors with Antitumor Activity. *J. Med. Chem.* **2015**, *58* (1), 433−442.
(15) Castanedo, G.; Clark, K.; Wang, S.; Tsui, V.; Wong, M.; Nicholas, J.; Wickramasinghe, D.; Marsters, J. C.; Sutherlin, D. CDK2/CyclinA Inhibitors: Targeting the CyclinA Recruitment Site with Small Molecules Derived from Peptide Leads. *Bioorg. Med. Chem. Lett.* **2006**, *16* (6), 1716−1720.
(16) McInnes, C.; Andrews, M. J. I.; Zheleva, D. I.; Lane, D. P.; Fischer, P. M. Peptidomimetic Design of CDK Inhibitors Targeting the Recruitment Site of the Cyclin Subunit. *Curr. Med. Chem.: Anti-Cancer Agents* **2003**, No. 1, 57−69.
(17) Bair, K. W.; Chen, Y-N. P.; Ramsey, T. M.; Sabio, M. L.; Sharma, S. K. Novartis-Erfindungen verwaltungsgesellschaft M.B.H. Inhibitors of the E2F-1/Cyclin Interaction for Cancer Therapy. WO2002050102A2 2002.
(18) Boehm, M.; Beaumont, K.; Jones, R.; Kalgutkar, A. S.; Zhang, L.; Atkinson, K.; Bai, G.; Brown, J. A.; Eng, H.; Goetz, G. H.; Holder, B. R.; Khunte, B.; Lazzaro, S.; Limberakis, C.; Ryu, S.; Shapiro, M. J.; Tylaska, L.; Yan, J.; Turner, R.; Leung, S. S. F.; Ramaseshan, M.; Price, D. A.; Liras, S.; Jacobson, M. P.; Earp, D. J.; Lokey, R. S.; Mathiowetz, A. M.; Menhaji-Klotz, E. Discovery of Potent and Orally Bioavailable Macrocyclic Peptide−Peptoid Hybrid CXCR7 Modulators. *J. Med. Chem.* **2017**, *60* (23), 9653−9663.
(19) Everaert, K.; Holm-larsen, T.; Kheir, G. B.; Rottey, S.; Weiss, J.; Walle, J. V.; Kabarriti, A.; Dossche, L.; Hervé, F.; Spinoit, A.-F.; Nørgaard, J. P.; Juul, K. Potential Clinical Applications of Current and Future Oral Forms of Desmopressin (Review). *Exp. Ther. Med.* **2024**, *28* (2), No. 303, DOI: 10.3892/etm.2024.12592.
(20) Xu, D.; Lan, C.; Kou, J.; Yao, S.; Zhao, W.; Kendrick, K. M. Oromucosal Administration of Oxytocin: The Development of 'Oxipops'. *Pharmaceutics* **2024**, *16* (3), 333.
(21) Peterlin Masic, L. Arginine Mimetic Structures in Biologically Active Antagonists and Inhibitors. *Curr. Med. Chem.* **2006**, *13* (30), 3627−3648.
(22) Rewinkel, J. M.; Adang, A. E. Strategies and Progress towards the Ideal Orally Active Thrombin Inhibitor. *Curr. Pharm. Des.* **1999**, *5* (12), 1043−1075.
(23) Rand, A. C.; Leung, S. S. F.; Eng, H.; Rotter, C. J.; Sharma, R.; Kalgutkar, A. S.; Zhang, Y.; Varma, M. V.; Farley, K. A.; Khunte, B.; Limberakis, C.; Price, D. A.; Liras, S.; Mathiowetz, A. M.; Jacobson, M. P.; Lokey, R. S. Optimizing PK Properties of Cyclic Peptides: The Effect of Side Chain Substitutions on Permeability and Clearance. *MedChemComm* **2012**, *3* (10), 1282−1289.
(24) Matsson, P.; Doak, B. C.; Over, B.; Kihlberg, J. Cell Permeability beyond the Rule of 5. *Adv. Drug Delivery Rev.* **2016**, *101*, 42−61.
(25) Caron, G.; Kihlberg, J.; Goetz, G.; Ratkova, E.; Poongavanam, V.; Ermondi, G. Steering New Drug Discovery Campaigns: Permeability, Solubility, and Physicochemical Properties in the bRo5 Chemical Space. *ACS Med. Chem. Lett.* **2021**, *12* (1), 13−23.
(26) ClinicalTrials.gov ID NCT06577987.
(27) Andrews, M. J. I.; McInnes, C.; Kontopidis, G.; Innes, L.; Cowan, A.; Plater, A.; Fischer, P. M. Design, Synthesis, Biological Activity and Structural Analysis of Cyclic Peptide Inhibitors Targeting the Substrate Recruitment Site of Cyclin-Dependent Kinase Complexes. *Org. Biomol. Chem.* **2004**, *2* (19), 2735.
(28) Singh, S.; Gleason, C. E.; Fang, M.; Laimon, Y. N.; Khivansara, V.; Xie, S.; Durmaz, Y. T.; Sarkar, A.; Ngo, K.; Savla, V.; Li, Y.; Abu-Remaileh, M.; Li, X.; Locquet, M.-A.; Tuladhar, B.; Odeh, R.; Hamkins-Indik, F.; He, D.; Membreno, M. W.; Nosrati, M.; Gushwa,

N. N.; Leung, S. S. F.; Fraga-Walton, B.; Hernandez, L.; Baldomero, M. P.; Lent, B. M.; Spellmeyer, D.; Luna, J. F.; Hoang, D.; Gritsenko, Y.; Chand, M.; DeMart, M. K.; Metobo, S.; Bhatt, C.; Shapiro, J. A.; Yang, K.; Dupper, N. J.; Bockus, A. T.; Fang, J.; Bambal, R.; Cremin, P.; Doench, J. G.; Aggen, J. B.; Liu, L.-F.; Levin, B.; Wang, E. W.; Vendrell, I.; Fischer, R.; Kessler, B.; Gokhale, P. C.; Signoretti, S.; Spektor, A.; Kreatsoulas, C.; Evangelista, M.; Singh, R.; Earp, D. J.; Nijhawan, D.; Garcia, P. D.; Oser, M. G. Targeting G1−S-checkpoint-compromised cancers with cyclin A/B RxL inhibitors. *Nature* **2025**, in press.

(29) Kontopidis, G.; Andrews, M. J. I.; McInnes, C.; Cowan, A.; Powers, H.; Innes, L.; Plater, A.; Griffiths, G.; Paterson, D.; Zheleva, D. I.; Lane, D. P.; Green, S.; Walkinshaw, M. D.; Fischer, P. M. Insights into Cyclin Groove Recognition. *Structure* **2003**, *11* (12), 1537−1546.

(30) Chatterjee, J.; Laufer, B.; Kessler, H. Synthesis of N-Methylated Cyclic Peptides. *Nat. Protoc.* **2012**, *7* (3), 432−444.

(31) Liras, S.; McClure, K. F. Permeability of Cyclic Peptide Macrocycles and Cyclotides and Their Potential as Therapeutics. *ACS Med. Chem. Lett.* **2019**, *10* (7), 1026−1032.

(32) Naylor, M. R.; Bockus, A. T.; Blanco, M.-J.; Lokey, R. S. Cyclic Peptide Natural Products Chart the Frontier of Oral Bioavailability in the Pursuit of Undruggable Targets. *Curr. Opin. Chem. Biol.* **2017**, *38*, 141−147.

(33) Digiesi, V.; Roque, V. d. l. O.; Vallaro, M.; Caron, G.; Ermondi, G. Permeability Prediction in the Beyond-Rule-of 5 Chemical Space: Focus on Cyclic Hexapeptides. *Eur. J. Pharm. Biopharm.* **2021**, *165*, 259−270, DOI: 10.1016/j.ejpb.2021.05.017.

(34) Rezai, T.; Yu, B.; Millhauser, G. L.; Jacobson, M. P.; Lokey, R. S. Testing the Conformational Hypothesis of Passive Membrane Permeability Using Synthetic Cyclic Peptide Diastereomers. *J. Am. Chem. Soc.* **2006**, *128* (8), 2510−2511.

(35) Schwochert, J.; Turner, R.; Thang, M.; Berkeley, R. F.; Ponkey, A. R.; Rodriguez, K. M.; Leung, S. S. F.; Khunte, B.; Goetz, G.; Limberakis, C.; Kalgutkar, A. S.; Eng, H.; Shapiro, M. J.; Mathiowetz, A. M.; Price, D. A.; Liras, S.; Jacobson, M. P.; Lokey, R. S. Peptide to Peptoid Substitutions Increase Cell Permeability in Cyclic Hexapeptides. *Org. Lett.* **2015**, *17* (12), 2928−2931.

(36) Beck, J. G.; Chatterjee, J.; Laufer, B.; Kiran, M. U.; Frank, A. O.; Neubauer, S.; Ovadia, O.; Greenberg, S.; Gilon, C.; Hoffman, A.; Kessler, H. Intestinal Permeability of Cyclic Peptides: Common Key Backbone Motifs Identified. *J. Am. Chem. Soc.* **2012**, *134* (29), 12125−12133.

(37) White, T. R.; Renzelman, C. M.; Rand, A. C.; Rezai, T.; McEwen, C. M.; Gelev, V. M.; Turner, R. A.; Linington, R. G.; Leung, S. S. F.; Kalgutkar, A. S.; Bauman, J. N.; Zhang, Y.; Liras, S.; Price, D. A.; Mathiowetz, A. M.; Jacobson, M. P.; Lokey, R. S. On-Resin N-Methylation of Cyclic Peptides for Discovery of Orally Bioavailable Scaffolds. *Nat. Chem. Biol.* **2011**, *7* (11), 810−817.

(38) Kelly, C. N.; Townsend, C. E.; Jain, A. N.; Naylor, M. R.; Pye, C. R.; Schwochert, J.; Lokey, R. S. Geometrically Diverse Lariat Peptide Scaffolds Reveal an Untapped Chemical Space of High Membrane Permeability. *J. Am. Chem. Soc.* **2021**, *143* (2), 705−714.

(39) Bockus, A. T.; McEwen, C. M.; Lokey, R. S. Form and Function in Cyclic Peptide Natural Products: A Pharmacokinetic Perspective. *Curr. Top. Med. Chem.* **2013**, *13* (7), 821−836.

(40) Leung, S. S. F.; Mijalkovic, J.; Borrelli, K.; Jacobson, M. P. Testing Physical Models of Passive Membrane Permeation. *J. Chem. Inf. Model.* **2012**, *52* (6), 1621−1636.

(41) Li, Y.; Li, W.; Xu, Z. Improvement on Permeability of Cyclic Peptide/Peptidomimetic: Backbone N-Methylation as A Useful Tool. *Mar. Drugs* **2021**, *19* (6), 311.

(42) Naylor, M. R.; Ly, A. M.; Handford, M. J.; Ramos, D. P.; Pye, C. R.; Furukawa, A.; Klein, V. G.; Noland, R. P.; Edmondson, Q.; Turmon, A. C.; Hewitt, W. M.; Schwochert, J.; Townsend, C. E.; Kelly, C. N.; Blanco, M.-J.; Lokey, R. S. Lipophilic Permeability Efficiency Reconciles the Opposing Roles of Lipophilicity in Membrane Permeability and Aqueous Solubility. *J. Med. Chem.* **2018**, *61* (24), 11169−11182.

(43) Poongavanam, V.; Wieske, L. H. E.; Peintner, S.; Erdelyi, M.; Kihlberg, J. Molecular Chameleons in Drug Discovery. *Nat. Rev. Chem.* **2024**, *8*, 45−60.

(44) Bockus, A. T.; Schwochert, J. A.; Pye, C. R.; Townsend, C. E.; Sok, V.; Bednarek, M. A.; Lokey, R. S. Going out on a Limb: Delineating the Effects of β-Branching, N-Methylation, and Side Chain Size on the Passive Permeability, Solubility, and Flexibility of Sanguinamide A Analogues. *J. Med. Chem.* **2015**, *58* (18), 7409−7418.

(45) Summerfield, S. G.; Yates, J. W. T.; Fairman, D. A. Free Drug Theory − No Longer Just a Hypothesis? *Pharm. Res.* **2022**, *39* (2), 213−222.

(46) Di, L. An Update on the importance of plasma protein binding in drug discovery and development. *Expert Expert Opin. Drug Discovery* **2021**, *16* (12), 1453−1465.

(47) Peterson, M. L. The Evolution of Macrocycles in Drug Discovery: From Technologies to Drugs. *Am. Pharm. Rev.* **2017**, No. 343609.

NOTE ADDED AFTER ASAP PUBLICATION

The title of this article was updated after it was published ASAP August 14, 2025. The corrected version was posted August 20, 2025.

https://doi.org/10.1021/acs.jmedchem.5c00253
J. Med. Chem. 2025, 68, 17030−17045